$Ta_3N_5/Co(OH)_x$ composite as photocatalyst for photoelectrochemical water splitting

Kaiqi Xu[1], Athanasios Chatzitakis[1], Ingvild Julie Thue Jensen[2], Mathieu Grandcolas[2], Truls Norby[1]*

(1) Centre for Materials Science and Nanotechnology, Department of Chemistry, University of Oslo, FERMiO, Gaustadalléen 21, NO-0349 Oslo, Norway.

(2) SINTEF Industry, P.O. Box 124 Blindern, NO-0314 Oslo, Norway

[*]*corresponding author* truls.norby@kjemi.uio.no

Abstract

Ta_3N_5 nanotubes (NTs) were obtained from nitridation of Ta_2O_5 NTs, which were grown directly on Ta foil through a 2-step anodization procedure. With $Co(OH)_x$ decoration, a photocurrent density as high as 2.3 mA/cm^2 (1.23 V vs. NHE) was reached under AM1.5G simulated solar light, however, the electrode suffered from photocorrosion. More stable photoelectrochemical (PEC) performance was achieved by first loading $Co(OH)_x$, followed by loading cobalt phosphate (Co-Pi) as double co-catalysts. The $Co(OH)_x$/Co-Pi double co-catalysts may act as a hole storage layer that slows down the photocorrosion caused by the accumulated holes on the surface of the electrode. A "waggling" appearance close to the "mouth" of Ta_2O_5 NTs was observed, and may indicate a structural instability of the "mouth" region, which breaks into segments after nitridation and forms a top layer of broken Ta_3N_5 NTs. A unique mesoporous structure of the walls of the Ta_3N_5 NTs, which is here reported the first time, is also a result of nitridation process. We believe that the mesoporous structure

makes it difficult for the nanotubes to be fully covered by the co-catalysts layer, hence rationalizing remaining degradation by photocorrosion.

1. Introduction

Photoelectrochemical (PEC) water splitting is a promising method to produce hydrogen as a green energy carrier from solar light[1, 2]. Since the first demonstration water splitting on the surface of n-type TiO_2 as the photoanode[3], tremendous efforts have been made to increase the solar to hydrogen (STH) efficiency by new materials and cell configurations[4-6]. The central processes such as the light absorption and conversion via redox reactions take place on the photoelectrodes, hence the properties and structure of the photoelectrode materials play crucial roles. For a single photoelectrode PEC cell, a semiconductor with a bandgap close to 2.0 eV will be ideal for PEC water splitting, considering that overpotentials for red-ox reactions and ohmic losses through the cell are required in addition to the thermodynamic potential (1.23 eV[7]) required for water splitting . Preferably, the conduction band minimum (CBM) and valence band maximum (VBM) should straddle the water redox potentials, so that an external bias is not needed. Since the PEC water splitting is usually performed in an aqueous electrolyte, the material should also be long term stable in such an environment under solar illumination. As a consequence, all the bottom-line requirements mentioned above have already eliminated most of the common materials, such as TiO_2, which has too wide bandgap (3.2 eV for anatase[8]), CdS, which suffers from photocorrosion[9], and α-Fe_2O_3, of which the CBM is not negative enough to drive the hydrogen evolution half reaction[10].

Due to the suitable bandgap (2.1 eV) and appropriate band positions[11], Ta_3N_5 has been intensively studied[12, 13] as photoanode material for visible-light-driven PEC water splitting[14]. Its efficiency can be determined by three factors[15, 16], namely, the absorption efficiency of photons, the separation and transport of photo-generated charge carriers (electron and hole pairs), and the injection of the photo-generated holes from the surface into the absorbed

species. Therefore, strategies to improve the efficiency are also straightforward. For instance, nanostructure engineering is developed to increase not only the concentration of reaction sites but also the photon absorption efficiency[17, 18], doping and heterojunctions are employed to enhance the charge separation and transport[19, 20], and co-catalysts decoration is applied to improve the charge injection from the electrode to the surface states (absorbed species)[19]. Recently 1D Ta_3N_5 materials, such as nanotubes[21] and nanorods[22], have attracted attention due to their unique properties in charge transport and significantly increased surface area, which is usually in combination with the co-catalysts coating to further boost the solar light conversion efficiency[22-24].

This work focuses on 1D Ta_3N_5 nanotubes (NTs) as the main photoelectrode material due to the relative easiness to synthesize it and scale up. The synthesis of Ta_3N_5 NTs usually starts from the growth of Ta_2O_5 NTs by anodization, which is commonly used in growing other metal oxide nanotubes such as TiO_2 nanotubes[25-27]. The first generation of vertically oriented Ta_2O_5 NTs were grown on Ta foil by one-step anodization in an electrolyte containing a concentrated H_2SO_4 and HF mixture[28, 29]. This introduced quite violent electrochemical reactions during formation of the nanotube arrays, resulting in poor attachment between the nanotube arrays and the substrate. Although better adhesion was reported later by using less concentrated HF in the electrolyte[30], obtaining long and stable Ta_2O_5 NTs was still challenging. In recent years, Ta_2O_5 NTs grown by anodization in a concentrated H_2SO_4 and $NH_4F_{(aq)}$ mixture have shown good stability and high aspect ratio, and the nanotubes were preserved after high temperature nitridation in NH_3 gas environment in order to obtain Ta_3N_5 NTs[17, 18, 21, 31]. A photocurrent density as high as 7.5 mA/cm^2 was obtained for Ba-doped Ta_3N_5 NTs decorated with Co-Pi (cobalt phosphate) as the co-catalyst[31]. However, the stability of such high performance is questionable, since Ta_3N_5 suffers from photocorrosion[22],

and the stability of nanotube-based Ta_3N_5 photoanodes is rarely mentioned in the literature[18, 21, 30-32].

In this work, Ta3N5 NTs are synthesized with optimized parameters based on the procedure provided in the literature17, 18. Different Co-based co-catalysts are loaded on the Ta3N5 NTs in order to facilitate the hole transfer from the electrode to the surface states (absorbed species), so as to enhance the PEC water splitting performance. An attempt to improve the overall PEC water splitting stability is carried out by first depositing Co(OH)x, followed by depositing Co-Pi as double oxygen evolution reaction (OER) co-catalysts. The micro morphology of the Ta2O5 NTs and Ta3N5 NTs is studied and discussed. A "waggling" appearance close to the "mouth" of Ta2O5 NTs is observed in transmission electron microscopy (TEM), and a mesoporous structure on the walls of the Ta3N5 NTs resulting from nitridation is observed by scanning electron microscopy (SEM).

2. Experimental

2.1 Materials

Ta foil (0.25 mm thick, ≥99.9% purity, Sigma-Aldrich) was used as the substrate for the growth of Ta_2O_5 NTs. All the chemicals were of analytical grade from Sigma-Aldrich and used as received. Deionized water (18.2 MΩ cm) was used for the preparation of all the solutions. NH_3 (standard cooling quality, ≥ 99.92%) and N_2 5.0 were both obtained from Praxair.

2.2 Preparation of Ta_3N_5 NTs

The preparation procedure of Ta_3N_5 NTs is schematically given in Fig. 1. The synthesis of Ta_3N_5 NTs starts from the growth of vertically aligned Ta_2O_5 NTs on a piece of Ta foil through a two-step anodization, with optimized parameters based on previously reported methods[17, 21, 30, 33]. The Ta foil was cut and cleaned by sonication in a sequence of acetone,

isopropanol and DI H_2O and dried under a N_2 flow. The first layer was grown under 60 V for 30 min in a diluted sulfuric acid electrolyte (H_2SO_4, 98% : H_2O vol. = 6.35) which contained 0.8 wt.% of NH_4F, and subsequently was removed by applying a Scotch® tape. A second nanotube layer was grown under the same anodization procedure, and was stabilized by immersing the electrode in absolute ethanol for 5 min after anodization[18]. The obtained Ta_2O_5 NTs were annealed in a continuous NH_3 flow (15 sccm) in a ProboStat™, which provided good control of the gas environment under high temperature. The Ta_2O_5 NTs were first heated up to 950 °C in a continuous N_2 flow with a ramping rate of 5 °C/min, after which the N_2 was switched to NH_3 for 2 h at 950 °C, followed by a cooling process with a cooling rate of 5 °C/min under the flow of NH_3.

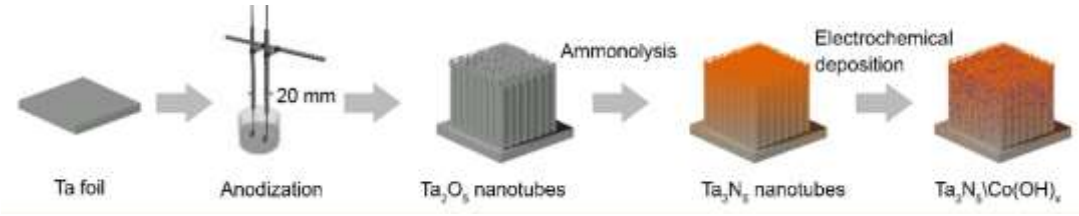

Figure 1. *Preparation procedure for bare Ta_3N_5 NTs and Ta_3N_5/co-catalyst electrodes*

2.3 Loading of co-catalysts

The $Co(OH)_x$ co-catalyst was electrodeposited on Ta_3N_5 NTs according to the Pourbaix diagram of Co species[34]. A three-electrode electrochemical cell was used with Ta_3N_5 NTs as the working electrode, SCE as the reference electrode and Pt foil as the counter electrode. -0.5 V vs. SCE was applied on the working electrode for 60 s in a stirred solution containing 0.05 M $Co(NO_3)_2$, where the pH was adjusted to 11-12 by slowly adding 1 M NaOH. The pH of the solution was monitored by a pH meter (HORIBA D-71G, Japan).

Co-Pi was electrodeposited according to a previously published procedure[35] with slight modifications. In the present case, 0.85 V vs. SCE were applied for 60 s on the $Co(OH)_x$ loaded Ta_3N_5 NTs, which were immersed in a solution of 0.05 mM $Co(NO_3)_2$ at pH 7 (0.1 M potassium phosphate buffer), and dried in ambient air.

2.4 Characterization

The nanotubes were characterized in plane-view and cross-section by scanning electron microscopy (SEM, FEI 650 NOVA NanoSEM instrument) equipped with a secondary electron (SE) detector and operated at an acceleration voltage of 5 kV. Scanning transmission and transmission electron microscopy (S/TEM) of the nanotube cross-sections were carried out at 300 kV with an FEI Titan G2 60-300 instrument equipped with a DCOR probe Cs-aberration corrector, and a Super-X Bruker energy dispersive spectrometer with 4 silicon drift detectors. TEM imaging was carried out in bright field mode coupled to selected area electron diffraction (SAED). High-angle annular dark field (HAADF) imaging was performed with a probe current of ~100 pA and nominal spatial resolution of 0.08 nm. The crystal structure was analyzed using a Rigaku MiniFlex 600 XRD with a Cu(α) 1 radiation source (λ = 1.5046 Å), step 0.01° (2θ) and scan rate 1°/min. The existence of co-catalysts on the surface of the nanotubes was confirmed by X-ray photoelectron spectroscopy (XPS) using a Kratos Axis Ultra^{DLD} spectrometer, with monochromated Al Kα radiation (hν = 1486.6 eV). High resolution spectra were measured using step size 0.1 eV and pass energy 40 eV. The energy axis was calibrated using the position of the Ta 4f component of Ta_3N_5 at 25.0 eV[36]. Peak fitting was done after Shirley background subtraction[37] using the CasaXPS software.

2.5 PEC measurements

PEC measurements were conducted in an alkaline electrolyte containing 1 M NaOH with pH 13.6, using the same three-electrode configuration as for the electrodeposition of the co-catalysts. Before any measurement, the aqueous electrolyte was purged thoroughly with N_2 gas, in order to remove any dissolved oxygen that may contribute to the reduction reaction at the cathode. The photocurrent was recorded by a Gamry Reference 3000 potentiostat, under 1 sun simulated solar light using a Newport Oriel® LCS-100 solar simulator equipped with a 100 W ozone-free xenon lamp and an AM 1.5G filter. The illumination intensity was

calibrated regularly by a mono-crystalline Si PV reference cell (Newport 91150V-KG5). Potentials were corrected vs. NHE by using the Nernst equation: $E_{NHE} = E_{meas} + 0.059\ \mathrm{V} \times pH\ + 0.241\ \mathrm{V}$.

3. Results and discussions

Figure 2a shows a cross section SEM image of Ta_3N_5 NTs, where a 2-layer structure is clearly seen. The nanotube structure was well preserved from Ta_2O_5 NTs (Figure 2a, inset) after nitridation at 950 °C. The top layer of Ta_3N_5 NTs mostly consists of broken nanotubes, which have also been witnessed by other researchers[31], and reported to have no significant effect on the photocurrent[17]. The length of the more organized nanotubes in the second layer is ~14 μm, and appears to be mesoporous (Figure 2b), which is rarely reported in the literature and most likely is formed due to the aggressive nitridation process[13]. The average outer diameter of the nanotubes is ~120 nm, and the wall thickness is ~40 nm, as can be estimated from Figure 2c.

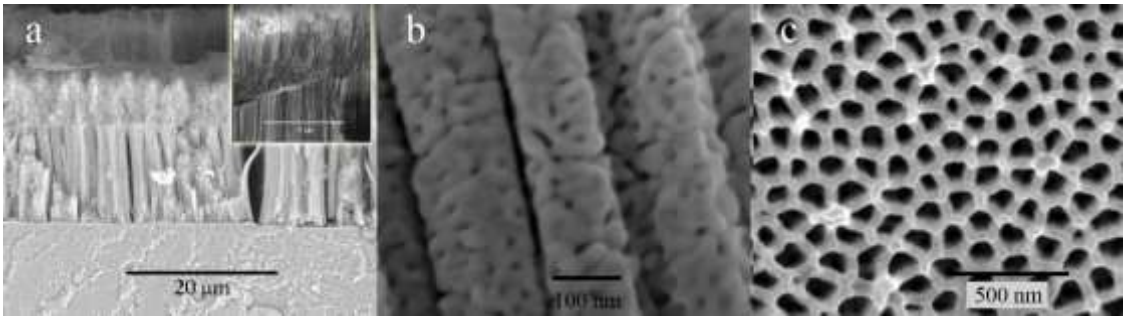

Figure 2. *SEM images of Ta_3N_5 NTs a) cross-sectional view, b) closer side view and c) top view. 2-layer mesoporous Ta_3N_5 NTs with an average length (second layer) of ~14 μm were aligned vertically on the Ta foil. The inset shows the cross-sectional SEM image of Ta_2O_5 NTs, indicating that the 2-layer nanotube structure was preserved after nitridation.*

Figure 3a-b shows TEM images of amorphous Ta_2O_5 NTs grown via anodization, where the average outer diameter and the wall thickness of the tubes is ~160 nm and ~55 nm, respectively. After nitridation, the outer diameter and the wall thickness of Ta_3N_5 NTs (Figure 3c) are found to be ~119 nm and ~42 nm, which are in good agreement with the dimensions obtained from SEM images. The slight shrinkage from Ta_2O_5 NTs to Ta_3N_5 NTs is a result of

nitridation, during which every 3 O atoms are replaced by 2 N atoms[18]. In addition, the inset in Figure 3a shows a quite smooth tube wall without any mesopores, which further confirms the mesoporous structure appearing later in the Ta_3N_5 NTs as a result of the nitridation process. The "mouth" of the Ta_2O_5 NTs array in Figure 3b exhibits a "waggling" appearance, which is also present in the singular nanotube TEM image (Figure 3a), and may correspond to the formation of the top layer, as shown in Figure 2a. A possible explanation may be based on the plastic flow model proposed for the growth of TiO_2 NTs by the same technique, where the newly formed oxide at the bottom of nanotubes is believed to be pushed to the wall and keep the tube growing[27, 38]. Therefore, it is reasonable to assume that the "mouth" of the nanotubes will suffer less pressure from adjacent nanotubes compared to the bottom, resulting in the difficulty to maintain the structure stability. The HRTEM image of Ta_3N_5 NTs in Figure 3d shows nice crystallization after nitridation, where the fringes with an interspace of 5.1 Å match well with the orthorhombic Ta_3N_5 (020) crystal planes. The XRD pattern matches that of Ta_3N_5 (COD ® ID1005006), and confirms the successful conversion of Ta_2O_5 to Ta_3N_5 at 950 °C for 2 h in NH_3, without any noticeable existence of any other phases.

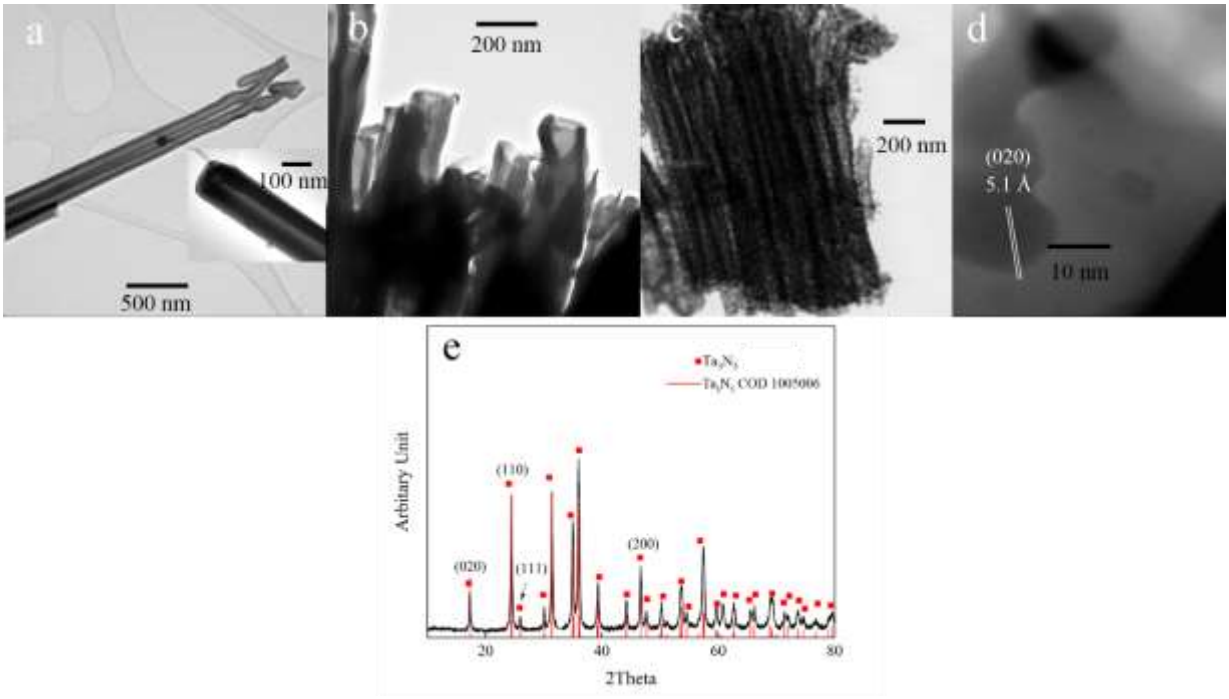

Figure 3 *TEM images of a) singular Ta_2O_5 nanotube, b) "mouth" of Ta_2O_5 NTs array, c) Ta_3N_5 NTs array, d) HAADF image showing Ta_3N_5 crystal where a mesoporous structure is present, and (020) planes can be clearly identified and e) XRD of fresh Ta_3N_5 NTs, peaks according to COD® crystallographic database with ID 1005006*

During the PEC water splitting process on an n-type semiconductor, the photo-generated holes should be transferred to the surface and subsequently injected into the surface states to participate in the oxygen evolution reaction. If the charge transfer suffers from sluggish kinetics, agglomerated holes may start oxidizing the material itself, leading to the decay of the photocurrent, which is a common drawback of nitride-based photoanodes[39]. A feasible and effective solution would be to modify the surface with a co-catalyst for oxygen evolution reaction (OER), e.g. IrO_2[40], Co_3O_4[41], Co-Pi[42], $Co(OH)_x$[43] and NiFe-LDH [22], so as to facilitate the charge transfer and (partially) prevent the photoanode from photocorrosion. Co-species based co-catalysts-Co-Pi and $Co(OH)_x$ were decorated on the Ta_3N_5 NTs by electrodeposition for efficient oxygen evolution.

To confirm the presence of Co (and P) species in the Ta_3N_5 NTs, XPS measurements were carried out. Figure 4 shows the Co 2p and P 2p regions for $Ta_3N_5/Co(OH)_x$ (Figure 4a), and $Ta_3N_5/Co(OH)_x$/Co-Pi (Figure 4b). The Co 2p peaks of both $Ta_3N_5/Co(OH)_x$ and $Ta_3N_5/Co(OH)_x$/Co-Pi are in close agreement to the $Co(OH)_2$ spectra reported by Biesinger *et al*.,[44] showing that the Co^{2+} state is dominant in both samples. However, for the $Ta_3N_5/Co(OH)_x$/Co-Pi sample, a P 2p peak is observed, at a peak position which is consistent with phosphate.[45] Co will be in the Co^{2+} state in both $Co(OH)_2$ and $Co_3(PO_4)_2$, which may be the reason why the Co 2p spectra are near identical for the sample with and without Co-Pi.

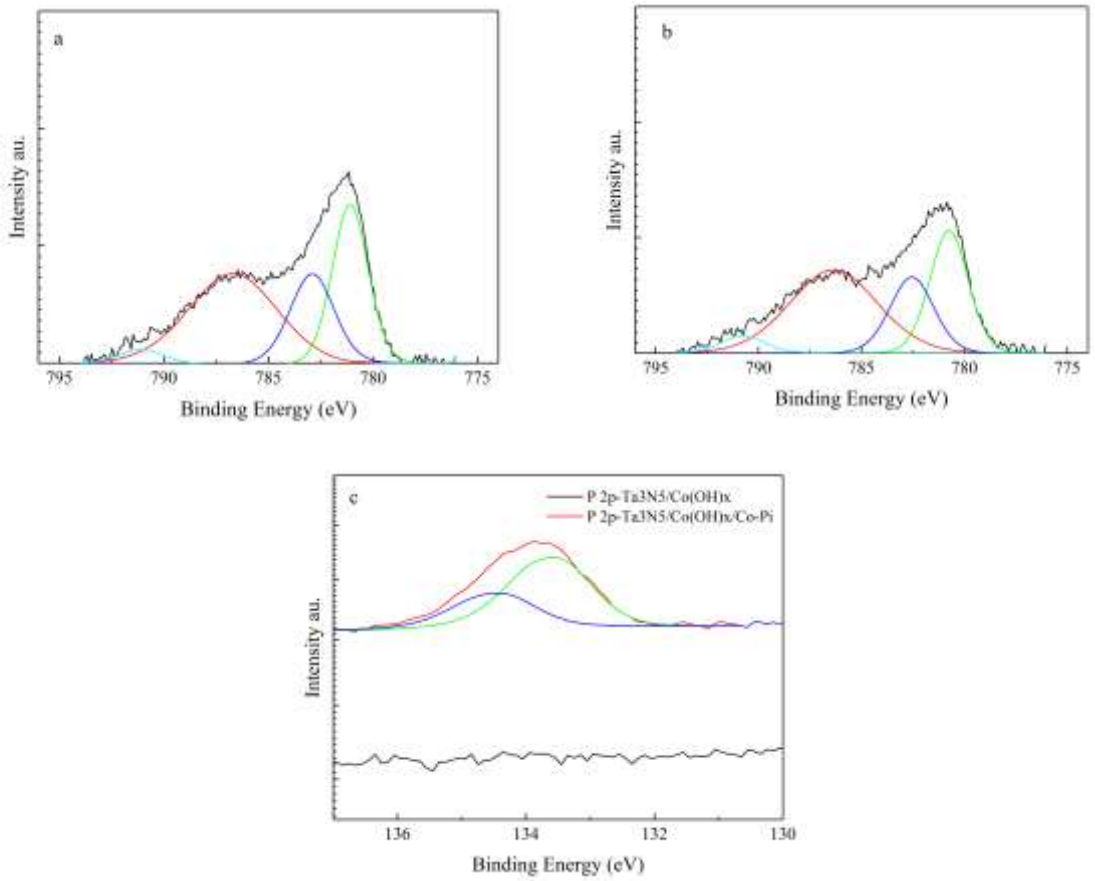

Figure 4 *XPS spectra of a) Co 2p from $Ta_3N_5/Co(OH)_x$, b) Co 2p from $Ta_3N_5/Co(OH)_x$/Co-Pi and c) P 2p from two electrodes*

Quantification of the sample content was performed based on the high resolution Ta 4f, Co 2p, P 2p, C 1s, O 1s and N 1s spectra, as presented in Table 1. Both samples have similar content of Ta, Co, C and N. The presence of P in $Ta_3N_5/Co(OH)_x$/Co-Pi is accompanied by a slight increase in O content. This could be consistent with the higher O content of $Co_3(PO_4)_2$ compared to $Co(OH)_2$.

Table 1 *Sample composition obtained from quantification of the high resolution XPS spectra.*

Sample	Ta at.%	Co at.%	P at.%	C at.%	O at.%	N at.%
$Ta_3N_5/Co(OH)_x$	25.7	2.0	0.0	10.5	23.7	38.2
$Ta_3N_5/Co(OH)_x$/Co-Pi	24.4	1.9	2.4	10.1	27.3	33.9

Figure 5a shows the *j-U* curves of different co-catalyst loaded Ta_3N_5 NTs, obtained from linear sweep voltammetry (LSV), under 1 sun simulated AM1.5G illumination with light on/off cycles. In order to make the comparison more reliable, results from the first LSV were not used. For the Co-Pi modified sample, the photocurrent at potential 1.23 V vs. NHE is 1.15 mA/cm^2, and for the $Co(OH)_x$ modified one it is 2.3 mA/cm^2, which are 10-fold and 20-fold increases, respectively, in photocurrent density compared to the bare Ta_3N_5. The sample $Ta_3N_5/Co(OH)_x$/Co-Pi obtained by first $Co(OH)_x$ deposition, followed by Co-Pi deposition shows similar photocurrent as $Ta_3N_5/Co(OH)_x$. However, chronoamperometry in Figure 5b shows that Ta_3N_5 NTs modified by both $Co(OH)_x$ and Co-Pi exhibit better photocurrent and stability at 1.15 V vs. NHE, starting from 0.85 mA/cm^2 and ending at 0.6 mA/cm^2, which represents a 30% degradation after 20 min. With only $Co(OH)_x$ decoration, the photocurrent starts from the same level but decays more than 50% after 20 min. When a more positive potential is applied, i.e. 1.65 V vs. NHE, the samples with only $Co(OH)_x$ or Co-Pi modification show very fast photocurrent degradation in the first few minutes. As a consequence, the photocurrent of $Ta_3N_5/Co(OH)_x$ becomes much lower than $Ta_3N_5/Co(OH)_x$/Co-Pi, in contrast to what is shown in the *j-U* plots (Figure 5a). Nevertheless, even with double co-catalysts loading, the material still experiences fast performance degradation when the applied potential is as positive as 1.65 V vs. NHE. The bare Ta_3N_5 NTs shows very small photocurrent throughout the chronoamperometry test, which is consistent with the literature[31].

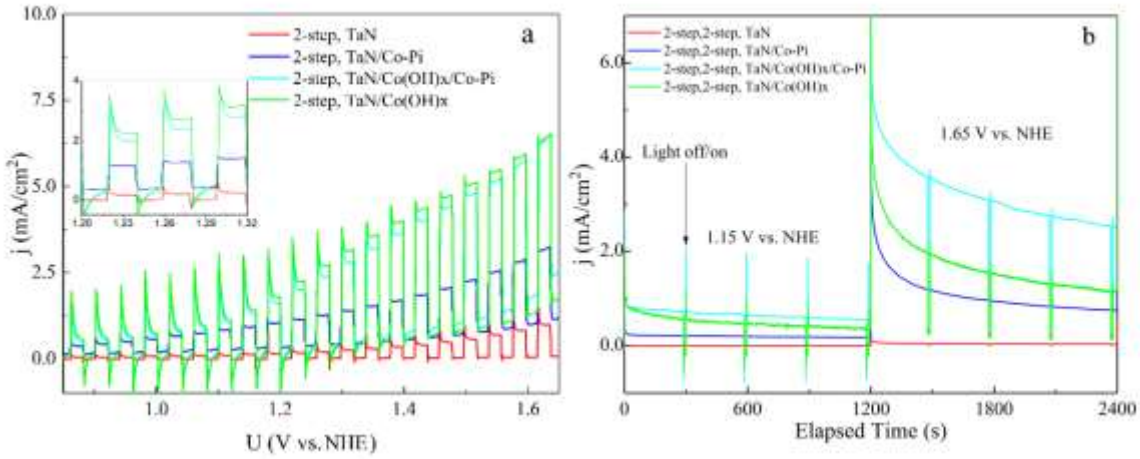

Figure 5. *a) j-U curves of bare Ta_3N_5, Ta_3N_5/Co-Pi, Ta_3N_5/$Co(OH)_x$, and Ta_3N_5/$Co(OH)_x$/Co-Pi under chopped AM1.5G simulated sunlight, in 1 M NaOH electrolyte, 10 mV/s scan rate and b) chronoamperometry of the same samples at 1.15 V vs. NHE and 1.65 V vs. NHE for 20 min each, with light on/off cycles*

The state-of-art photocurrent obtained from Ta_3N_5 NTs based photoanodes under simulated sunlight is 7.5 mA/cm^2 at 1.23 vs. NHE from Co-Pi modified, Ba doped nanotubes[31], and 6.3 mA/cm^2 at 1.23 vs. NHE from $Co(OH)_x$ modified, subnitrides introduced as the back contact of the nanotubes[18]. Although the highest photocurrent reported in this work is 2.3 mA/cm^2 vs. NHE, much less than the best performance in the literature, it should be mentioned that in order to have a more reliable photocurrent the best results obtained from first LSV was not used here. In addition, the stability of nanotube-based Ta_3N_5 photoanodes for PEC water splitting is rarely mentioned in the literature[17, 18, 21, 30, 31, 42], even though most of them claim photocurrent improvements at a certain applied potential. However, stable PEC water splitting performance by co-catalyst modified Ta_3N_5 synthesized in other morphologies have already been reported in the literature, such as Co-Pi modified Ta_3N_5 nanorods[23], Co-Pi+$Co(OH)_x$/NiFe-LDH multiple co-catalysts modified Ta_3N_5 nanorods[22] and ferrihydrite (Fh) protected Ta_3N_5 film[46]. However, to synthesize nanorods requires extra procedures and is usually more costly than nanotubes. The difficulty of maintaining the performance stability of Ta_3N_5 NTs compared to nanorods may result from the special morphology shown in the SEM and TEM images (Figures 2 and 3). The mesoporous structure makes it rather difficult to fully

cover the whole surface by co-catalysts during electrodeposition, hence photocorrosion takes place easily. Nevertheless, the results of this work may indicate one possible solution to further enhance the stability of nanotube-based Ta_3N_5 photoanodes. The $Co(OH)_x$/Co-Pi double co-catalysts may act as a hole storage layer similar to $Ni(OH)_x/MoO_3$[47], which efficiently harvests and stores the holes from Ta_3N_5 NTs. A pinhole free, high coverage ratio $Co(OH)_x$/Co-Pi layer may sufficiently enhance the stability, but better deposition parameters or a more appropriate deposition method are needed.

4. Conclusions

Ta_2O_5 nanotubes were grown directly on Ta foil by a 2-step anodization process. A "waggling" appearance of nanotubes close to the "mouth" was witnessed, which may result in the top layer consisting of broken nanotubes in the Ta_3N_5 NTs. A mesoporous structure all along the Ta_3N_5 NTs was observed, and was a consequence of the aggressive nitridation process. A high PEC activity was achieved by the Ta_3N_5 NTs with Co-based co-catalysts decoration. At an applied potential of 1.23 V vs. NHE, the photocurrent density reached 2.3 mA/cm^2 by $Co(OH)_x$ decorated Ta_3N_5 NTs under AM1.5G simulated solar light. With $Co(OH)_x$/Co-Pi double co-catalysts loading, the stability of PEC performance of Ta_3N_5 NTs at 1.15 V vs. NHE was >20% better than its counterparts, indicating the possibility to enhance the stability of nanotube-based Ta_3N_5 by loading multiple Co-species based OER co-catalysts. However, the unique mesoporous structure made it difficult to obtain a uniform coverage of co-catalysts on the nanotubes, resulting in the difficulty to maintain high PEC performance. Better deposition parameters or a more appropriate deposition method is needed to obtain a uniform and pin hole free $Co(OH)_x$/Co-Pi double co-catalyst layer, in order to further enhance the stability of Ta_3N_5 NTs.

Conflicts of interest

The author declares no conflicts of interest.

Acknowledgements

We are grateful to Dr. Patricia Almeida Carvalho (SINTEF) who helped with the SEM and TEM images. The work is funded by the Research Council of Norway under the NANO2021 program, project CO2BioPEC (250261).

References

1. R. J. Detz, J. N. H. Reek and B. C. C. van der Zwaan, *Energy Environ. Sci.*, 2018, DOI: 10.1039/C8EE00111A.
2. S. J. Moniz, S. A. Shevlin, D. J. Martin, Z.-X. Guo and J. Tang, *Energy Environ. Sci.*, 2015, **8**, 731-759.
3. A. Fujishima and K. Honda, *Nature*, 1972, **238**, 37-38.
4. R. v. d. Krol and M. Grätzel, *Photoelectrochemical hydrogen production*, Springer, New York, 2012.
5. H. J. Lewerenz, L. Peter and Royal Society of Chemistry (Great Britain), *Photoelectrochemical water splitting : materials, processes and architectures*, RSC Publishing, Cambridge, 2013.
6. Z. Chen, H. N. Dinh and E. Miller, *Photoelectrochemical water splitting : standards, experimental methods, and protocols*, Springer, New York, 2013.
7. M. Xiao, S. Wang, S. Thaweesak, B. Luo and L. Wang, *Engineering*, 2017, **3**, 365-378.
8. I. Tunc, M. Bruns, H. Gliemann, M. Grunze and P. Koelsch, *Surf. Interface Anal.*, 2010, **42**, 835-841.
9. D. Fermin, E. Ponomarev and L. Peter, *J. Electroanal. Chem.*, 1999, **473**, 192-203.
10. X. Chen, S. Shen, L. Guo and S. S. Mao, *Chem. Rev.*, 2010, **110**, 6503-6570.
11. W. J. Chun, A. Ishikawa, H. Fujisawa, T. Takata, J. N. Kondo, M. Hara, M. Kawai, Y. Matsumoto and K. Domen, *J. Phys. Chem. B*, 2003, **107**, 1798-1803.
12. C. Zhen, R. Chen, L. Wang, G. Liu and H.-M. Cheng, *J. Mater. Chem. A*, 2016, **4**, 2783-2800.
13. E. Nurlaela, A. Ziani and K. Takanabe, *Mater. Renew. Sustain. Energy*, 2016, **5**, 18.
14. P. Zhang, J. Zhang and J. Gong, *Chem. Soc. Rev.*, 2014, **43**, 4395-4422.
15. H. Dotan, K. Sivula, M. Gratzel, A. Rothschild and S. C. Warren, *Energy Environ. Sci.*, 2011, **4**, 958-964.
16. G. V. Govindaraju, G. P. Wheeler, D. Lee and K.-S. Choi, *Chem. Mater.*, 2017, **29**, 355-370.
17. L. Wang, N. T. Nguyen, X. Zhou, I. Hwang, M. S. Killian and P. Schmuki, *ChemSusChem*, 2015, **8**, 2615-2620.
18. L. Wang, X. Zhou, N. T. Nguyen, I. Hwang and P. Schmuki, *Adv. Mater.*, 2016, **28**, 2432-2438.
19. Y. Li, L. Zhang, A. Torres-Pardo, J. M. González-Calbet, Y. Ma, P. Oleynikov, O. Terasaki, S. Asahina, M. Shima and D. Cha, *Nat. Commun.*, 2013, **4**, 2566.
20. H.-i. Kim, D. Monllor-Satoca, W. Kim and W. Choi, *Energy Environ. Sci.*, 2015, **8**, 247-257.
21. L. Wang, A. Mazare, I. Hwang and P. Schmuki, *Electrochem. Commun.*, 2016, **72**, 27-31.
22. L. Wang, F. Dionigi, N. T. Nguyen, R. Kirchgeorg, M. Gliech, S. Grigorescu, P. Strasser and P. Schmuki, *Chem. Mater.*, 2015, **27**, 2360-2366.
23. Y. Li, T. Takata, D. Cha, K. Takanabe, T. Minegishi, J. Kubota and K. Domen, *Adv. Mater.*, 2013, **25**, 125-131.
24. J. Hou, Z. Wang, C. Yang, H. Cheng, S. Jiao and H. Zhu, *Energy Environ. Sci.*, 2013, **6**, 3322-3330.
25. K. Xu, A. Chatzitakis and T. Norby, *Photochem. Photobiol. Sci.*, 2017, **16**, 10-16.
26. A. Chatzitakis, M. Grandcolas, K. Xu, S. Mei, J. Yang, I. J. T. Jensen, C. Simon and T. Norby, *Catal. Today*, 2017, **287**, 161-168.

27. P. Roy, S. Berger and P. Schmuki, *Angew. Chem. Int. Ed.*, 2011, **50**, 2904-2939.
28. H. A. El-Sayed and V. I. Birss, *Nano Lett.*, 2009, **9**, 1350-1355.
29. N. K. Allam, X. J. Feng and C. A. Grimes, *Chem. Mater.*, 2008, **20**, 6477-6481.
30. X. Feng, T. J. LaTempa, J. I. Basham, G. K. Mor, O. K. Varghese and C. A. Grimes, *Nano Lett.*, 2010, **10**, 948-952.
31. Z. Su, S. Grigorescu, L. Wang, K. Lee and P. Schmuki, *Electrochem. Commun.*, 2015, **50**, 15-19.
32. S. Grigorescu, B. Bärhausen, L. Wang, A. Mazare, J. E. Yoo, R. Hahn and P. Schmuki, *Electrochem. Commun.*, 2015, **51**, 85-88.
33. Y. He, P. Ma, S. Zhu, M. Liu, Q. Dong, J. Espano, X. Yao and D. Wang, *Joule*, 2017, **1**, 831-842.
34. E. Garcia, J. Santos, E. Pereira and M. Freitas, *J. Power Sources*, 2008, **185**, 549-553.
35. D. K. Zhong, M. Cornuz, K. Sivula, M. Grätzel and D. R. Gamelin, *Energy Environ. Sci.*, 2011, **4**, 1759-1764.
36. Q. Gao, S. Wang, Y. Ma, Y. Tang, C. Giordano and M. Antonietti, *Angew. Chem.*, 2012, **124**, 985-989.
37. D. A. Shirley, *Physical Review B*, 1972, **5**, 4709.
38. D. Regonini, C. Bowen, A. Jaroenworaluck and R. Stevens, *Materials Science and Engineering: R: Reports*, 2013, **74**, 377-406.
39. C. Zhen, L. Wang, G. Liu, G. Q. M. Lu and H.-M. Cheng, *Chem. Commun.*, 2013, **49**, 3019-3021.
40. D. Yokoyama, H. Hashiguchi, K. Maeda, T. Minegishi, T. Takata, R. Abe, J. Kubota and K. Domen, *Thin Solid Films*, 2011, **519**, 2087-2092.
41. M. Liao, J. Feng, W. Luo, Z. Wang, J. Zhang, Z. Li, T. Yu and Z. Zou, *Adv. Funct. Mater.*, 2012, **22**, 3066-3074.
42. Y. Cong, H. S. Park, S. Wang, H. X. Dang, F.-R. F. Fan, C. B. Mullins and A. J. Bard, *The Journal of Physical Chemistry C*, 2012, **116**, 14541-14550.
43. M. Li, W. Luo, D. Cao, X. Zhao, Z. Li, T. Yu and Z. Zou, *Angew. Chem. Int. Ed.*, 2013, **52**, 11016-11020.
44. M. C. Biesinger, B. P. Payne, A. P. Grosvenor, L. W. Lau, A. R. Gerson and R. S. C. Smart, *Appl. Surf. Sci.*, 2011, **257**, 2717-2730.
45. M. W. Kanan and D. G. Nocera, *Science*, 2008, **321**, 1072-1075.
46. G. Liu, J. Shi, F. Zhang, Z. Chen, J. Han, C. Ding, S. Chen, Z. Wang, H. Han and C. Li, *Angew. Chem. Int. Ed.*, 2014, **53**, 7295-7299.
47. G. Liu, P. Fu, L. Zhou, P. Yan, C. Ding, J. Shi and C. Li, *Chem. Eur. J.*, 2015, **21**, 9624-9628.